01,02

Magnetic anisotropy of Nanostructured Fe-Ni−C Coating Produced by Electroless Deposition

© E.A. Denisova[1,2], L.A. Chekanova[1], S.V. Komogortsev[1,2,3], R.S. Iskhakov[1,3], O.A. Li[2], A.L. Sukhachev[1], D.A. Velikanov[1], I.V. Nemtsev[1,2,4]

[1] Kirensky Institute of Physics, Federal Research Center KSC SB, Russian Academy of Sciences, Krasnoyarsk, Russia
[2] Siberian Federal University, Krasnoyarsk, Russia
[3] Siberian State University of Science and Technology, Krasnoyarsk, Russia
[4] Krasnoyarsk Scientific Center of the Siberian Branch of the Russian Academy of Sciences, Krasnoyarsk, Russia

E-mail: len-den@iph.krasn.ru

Received April 17, 2023
Revised April 17, 2023
Accepted May 11, 2023

The structural and magnetic properties of nanostructured $Fe_{100-x}Ni_x$-C ($0 < x < 100$) coatings produced by electroless plating with different carbohydrates as reducing agents have been investigated. The phase-structural state of the films was studied by diffraction and electron microscopy. The Ni concentration ranges of FCC and BCC phases existence in electroless deposited films were determined. The surface morphology, saturation magnetization, local magnetic anisotropy field and coercivities of films are dependent on the iron content and type of reducing agent. The correlation between coercivity H_c and the anisotropy field of the magnetic stochastic domain which were established by correlation magnetometry suggests that the magnitude of H_c is mainly determined by this anisotropy.

Keywords: 3d-metal alloys, the approach to saturation magnetization law, coercivity.

DOI: 10.21883/PSS.2023.06.56090.14H

1. Introduction

Much attention is now being paid to the development of methods for preparing magnetic materials with high saturation induction for various applications, such as high-density fast magnetic recording heads, in microelectronic devices, radiation protection systems and others [1–4].

Alloys Fe-Ni — a well-known material for such applications — are made by a variety of methods [5,6]. Chemical deposition has a number of advantages, such as low cost, scalability to large areas, and the ability to coat curved surfaces. Current work here continues with the search for new non-toxic reductants. Polysaccharide reduction — a new approach resulting in the final nanostructured coatings containing free-form carbon [7]. The structure and magnetic properties of the coatings produced by this approach need to be examined.

Magnetic anisotropy of nanomaterials has been intensively studied as a major factor determining their magnetic properties [8,9]. The problem of experimental study of magnetic anisotropy and its relation to properties is quite complex, as it has proven important to consider magnetic anisotropy localized at different scales, from sample size to crystallite size. Magnetic softness in nanostructured alloys has been successfully explained by the random magnetic anisotropy model [10,11]. In addition to the magnetic anisotropy constant (field) of the crystallite (local magnetic anisotropy), the exchange interaction constant A, saturation magnetization M_s, crystallite size (correlation size of local axis of light magnetization) $2R_c$ are key in this model. The magnetic microstructure of amorphous and nanocrystalline alloys, in addition to the classical elements (domain, domain wall), is characterized by a new scale unit — a stochastic magnetic domain or magnetic orientation correlation length area [12,13]. The macroscopic magnetic characteristics of nanomagnetics, including characteristics important for applications, are largely due to the size R_L and anisotropy of $\langle K \rangle_L$ of these domains.

In the present study, the magnetic anisotropy of Fe-Ni−C alloys synthesized by chemical deposition using carbohydrates as reducing agents and its correlation with the features of their atomic and micromagnetic structure is studied.

2. Experiment

Three series $Fe_{100-x}Ni_x$-C ($0 < x < 100$) coatings have been synthesized by chemical deposition on copper and glass substrates using the following carbohydrates as reducing agents: arabinogalactan (series A); starch (series B); sucrose (series C). The coating deposition solution comprised metal salts (nickel sulfate $NiSO_4 \cdot 7H_2O$ and Mohr's

salt $Fe(NH_4)_2(SO_4)_2 \cdot 7H_2O$); sodium citrate $Na_3C_6H_5O_7$) and one of the reducing agents were used as a complexing and buffering agent. The precipitation was carried out at 80°C and the pH value was maintained by adding NaOH solution. Coatings with a thickness from 0.6 to 4 μm were obtained.

Synthesized samples were studied by electron microscopy (S5500 and TM3000 Hitachi scanning microscopes with an attachment for energy-dispersive analysis) and X-ray diffraction (DRON 3). The chemical composition of the samples was determined by the method of energy-dispersive analysis. The temperature and field dependences of the magnetization were measured on a vibrating magnetometer [14] and VSM 8604 (Lake Shore Cryotronics). Magnetic characteristics of synthesized materials (saturation magnetization, exchange interaction constant, coercivity) were studied as a function of the Fe, Ni and C content in the alloy. The characteristics of the magnetic microstructure — the magnitude of the local anisotropy field (H_a), the correlation radius of this anisotropy, the stochastic domain anisotropy field ($\langle H_a \rangle$) were determined by correlation magnetometry [13].

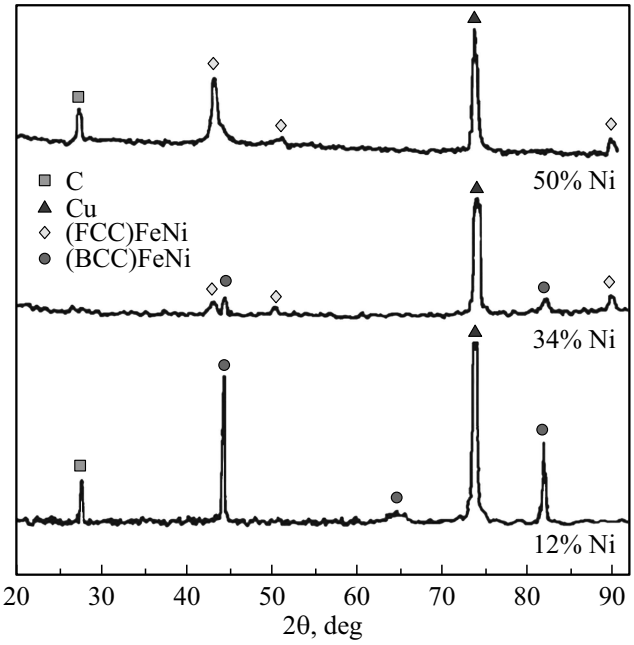

Figure 2. Diffraction patterns of Fe-Ni−C coatings with different Ni content.

3. Results and discussion

Varying the composition of the bath for chemical deposition (Fe:Ni ratio, the type of reducing agent) enables to synthesize Fe-Ni−C coatings with a thickness of up to 4 μm with a uniform distribution of elements, with the ability to control surface morphology and grain size (15−300 nm). Fig. 1 shows SEM images of the surface and cross-section of Fe-Ni−C films. As in the case of FeCo-C alloys reduced with carbohydrates [15], the most developed surface with pyramidal grains is characteristic of the alloy Fe-Ni−C deposited with sucrose as reducing agent. The films obtained by reduction with arabinogalactan had a smoothed surface. A cross section of the coating Fe-Ni−C (Fig. 1, *d*) shows that sucrose reduced coatings are characterized by columnar growth. X-ray diffraction spectra of Fe-Ni−C coatings with different nickel contents are shown in Fig. 2. We have found that films synthesized by chemical deposition with different reducing agents — carbohydrates, with the same chemical composition, have a similar crystalline structure. For all sample series, the alloy films $Fe_{100-x}Ni_x$ at $x < 12$ are a nanocrystalline body-centered cubic (BCC) solid solution, at $12 < x < 40$ a mixture of BCC and face-centered cubic (FCC) phases and at $x > 40$ a FCC phase solid solution.

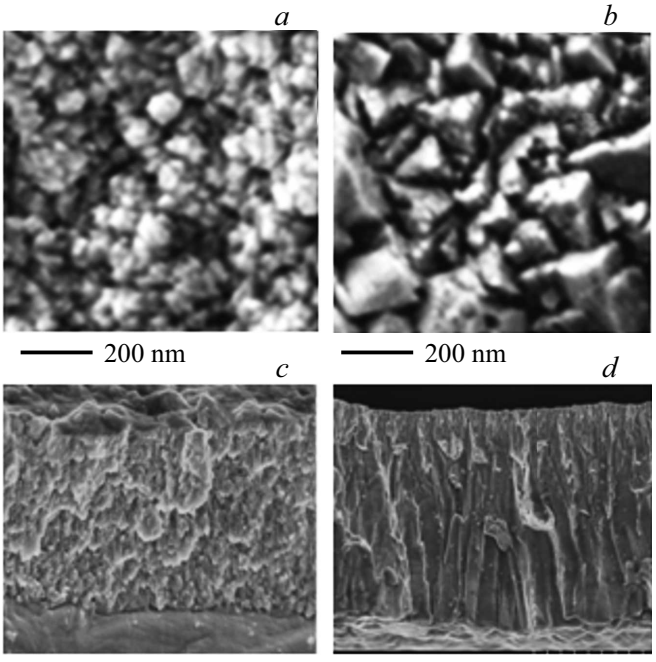

Figure 1. SEM surface and cross sectional images of Fe-Ni−C coatings obtained with different reducing agents: *a, c* — arabinogalactan, *b, d* — saccharose.

The crystallite size estimated by the Scherrer formula varies for all types of reducing agents within 10−27 nm. The composition of the alloy $Fe_{100-x}Ni_x$−C determines the value of the specific saturation magnetization σ_s of the samples tested. The σ_s value at $x = 10$ is 190 (Series A) and 180 $A \cdot m^2/kg$ (Series B and C); at $x = 40$ — the σ_s is around 105 (Series C) and 97 $A \cdot m^2/kg$ (Series A). The concentration dependence σ_s obtained in our paper is qualitatively the same as that for bulk alloys Fe-Ni [16]; the smaller σ_s values in our case are due to the presence of carbon in the $Fe_{100-x}Ni_x$−C coating. The low-temperature behavior of the saturation magnetization M_s in the coatings obeys Bloch's law $T^{3/2}$: $M_s(T) = M_{s0} \cdot (1 - B \cdot T^{3/2})$,

which allowed us to estimate the exchange constant as

$$A = \frac{k_B}{8\pi}\left(\frac{M_{S0}}{g\mu_B}\right)^{1/3}\left(\frac{2.612}{B}\right)^{2/3}.$$

The exchange constant for all sample series is in the range $(0.35-0.95)\cdot 10^{-6}$ erg/cm.

Information on the local magnetic anisotropy field H_a was obtained by studying the magnetization approach to saturation. The curves of magnetization approximation to saturation in all series of coatings for all values x are characterized by the Akulov dependence $M(H) \propto H^{-2}$ in fields larger than 2–6 kOe, which allowed to calculate for these alloys the value of the rms fluctuation of the local magnetic anisotropy field aH_a ($H_a = 2K/M_s$ — the local magnetic anisotropy field, the coefficient a — the symmetrical numerical coefficient for uniaxial anisotropy equal to $a = \sqrt{1/15}$, for cubic — $a = \sqrt{2/105}$). Fig. 3, *a* shows the experimental magnetization curves for films Fe-Ni–C with different content of Ni, plotted on double logarithmic scale,

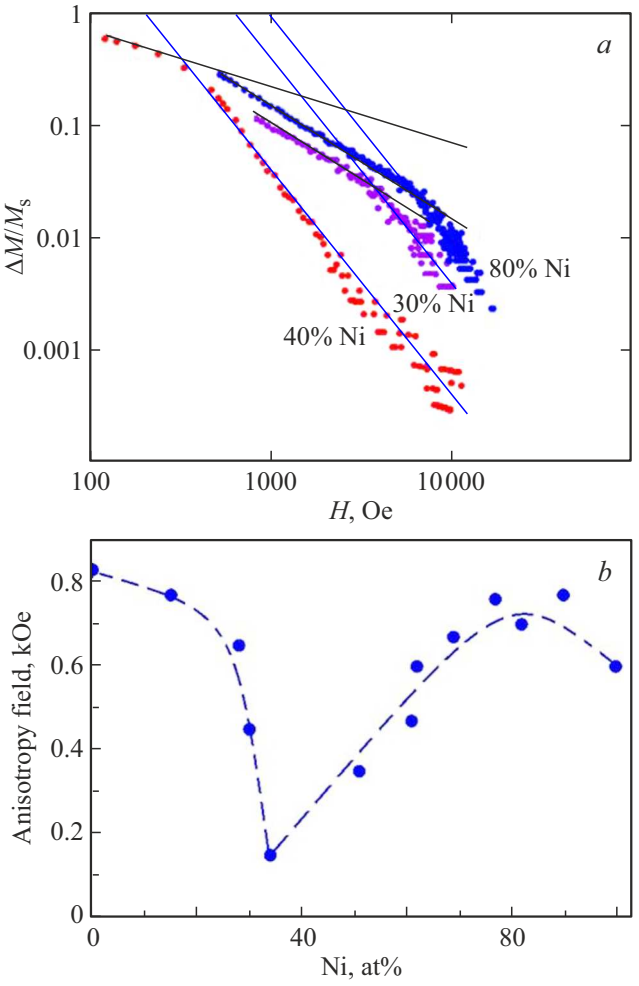

Figure 3. *a*) Saturation magnetization dispersion for Fe-Ni–C series C films with different Ni content; *b*) dependence of local anisotropy field on Ni content for Fe-Ni–C series C films.

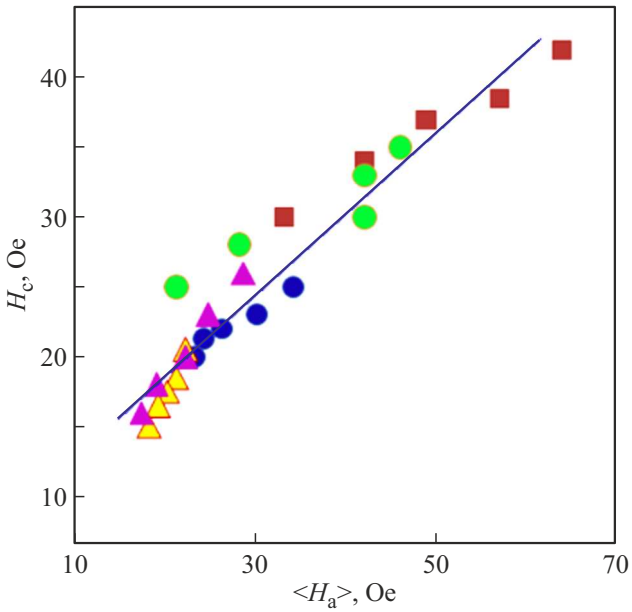

Figure 4. Dependence of coercive force of Fe-Ni–C films measured at different temperatures on the stochastic domain anisotropy field. Series B — with Ni 34% (crimson triangles), 61% (green circles), Series C — with Ni 24% (yellow triangles), 37% (blue circles), 49% (squares).

the lines in the diagram — fitting according to the equation $M = M_s \cdot (1 - (a \cdot H_a/H)^2)$ with coefficient $a = \sqrt{1/15}$.

The concentration dependence of the local anisotropy field $a^{0.5}H_a$ (containing magnetic crystallographic anisotropy and internal stress anisotropy contributions) forFe-Ni–C films is shown in Fig. 3, *b*. The observed minimum at 34% Ni is a consequence of the proximity of the alloy composition to invar. The dependence above does not show a decrease in H_a at the concentration of Ni typical of permalloy, which suggests that the main contribution to local anisotropy is made by magnetostatic interaction — anisotropy induced by magnetization inhomogeneities, rather than crystallographic anisotropy or internal stress anisotropy. In the range 1–3 kOe, magnetization approximation to saturation is carried out as $M(H) \propto H^{-\alpha}$. The exponent α is related to the effective dimensionality of the magnetic microstructure in a given field range.

The magnitude of the field $H_R = 2A/MR_c^2$ at which the power-law dependence changes allows to estimate the magnitude of the correlation radius of the random anisotropy R_c. Values R_c lie within the range 6–23 nm for all coating series. Note also, that increasing Ni content causes growth of R_c, i. e. in the case of nanostructured alloy Fe-Ni–C, it can be stated that grain size decreases with growing Fe:Ni ratio, which agrees with electron microscopy and X-ray diffraction analysis data. As the field decreases in the area of fields $H < H_R = 2A/MR_c^2$, the functional form of the curve $M(H)$ changes. These changes are associated with the occurrence and propagation of exchange-correlated

magnetization deviations („magnetization ripple“) in the spin system. In paper [17], it is shown that in exchange-correlated systems with random anisotropy the ripple length $R_H = (2A/MH)^{1/2}$ is bounded from below and above: $R_c \le R_H \le R_L$. Therefore, the functional dependence $M(H)$ in $H_L = 2A/MR_L^2 < H < H_R = 2A/MR_c^2$ field area can be determined from the expression

$$M = M_s\left(1 - (a \cdot H_a/H)^2\right), \qquad (1)$$

in which, the local anisotropy of particle H_a is replaced by the effective anisotropy of the area captured by a single ripple length R_H:

$$\frac{M_s - M}{M_s} = \frac{(aH_a)^2}{H_R^{d/2}} \cdot \frac{1}{H^{(4-d)/2}} = \frac{(a\langle H_a\rangle_L)^2}{H_L^{d/2}} \cdot \frac{1}{H^{(4-d)/2}}, \quad H_L < H < H_R \qquad (2)$$

Here, d — the packing dimension of ferromagnetic grains, $\langle H_a\rangle_L = 2\langle K\rangle_L/M_s$ — the field of macroscopic anisotropy in the stochastic domain. Fig. 4 shows the dependence of the coercive force, measured at different temperatures, on the anisotropy field of the stochastic domain. The observed correlation of these quantities suggests that the value H_c is mainly determined by this anisotropy.

The samples studied show a hysteresis loop shape non-typical of films, characterized by a smaller rectangularity and residual magnetization ($M_r/M_s \approx 0.6$). This reduction in the rectangularity of the hysteresis loop may be due to additional anisotropy introduced by the columnar microstructure of the film [18,19]. The perpendicular magnetic anisotropy field of films H_{pa} (at film thickness $L > L_{cr} = 2\pi(A/K_p)^{0.5}$) and its heterogeneity (histograms of grain distribution by values H_{pa}) have been assessed by fitting the descending branch of the hysteresis loop [20] (Fig. 5).

According to Stoner–Wohlfarth model, the saturation field in the direction perpendicular to the lightest magnetization axis is equal to the magnetic anisotropy field. The shape of the loop in this direction within the model represents a linear hysteresis-free magnetization dependence in the range from $-H_s$ ($M = -M_s$) to H_s ($M = M_s$); outside this range the sample is homogeneously magnetized to saturation ($M = \pm M_s$). In the experiment in the homogeneous film, a feature near the field $H_s = H_a$ is observed as a sharp break in the dependence $M(H)$. The heterogeneity of the anisotropy field blurs the break at $M(H)$ near H_s; this can be used to quantify not only the magnitude but also the heterogeneity of the magnetic anisotropy field.

The descending part of the hysteresis loop was approximated by the sum of the curves (Fig. 5):

$$M = \sum_i \left(M_r + H\frac{1 - M_r}{H_{si}}\right) \cdot N_i \qquad (3)$$

at magnetic field strengths less than H_s and $M = M_s$ in fields greater than H_{si}, where M_s — saturation magnetization and

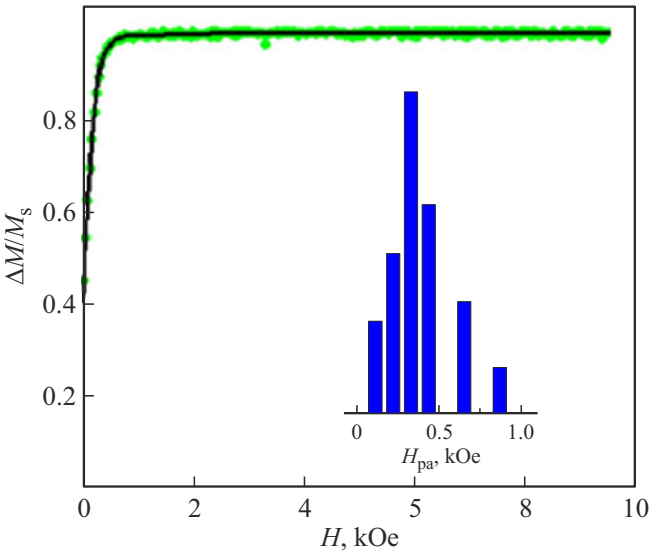

Figure 5. The descending branch of the hysteresis loop of the film Fe-Ni–C Series B; the insert shows the corresponding histogram of the grain distribution according to values H_{pa}.

H_{si} — saturation field strength i-th grain fraction, N_i — grain fraction. Thus, the simulation found the saturation fields of grains H_{si} and the proportion of N_i grains with a given value H_{si}.

The saturation field H_s is related to the magnetic constants and film parameters by the equation [20]:

$$1 - \frac{H_s}{H_{pa}} = 2\pi\sqrt{\frac{2A}{H_{pa}M_s}} \cdot L^{-1}\left[1 + \frac{H_{pa}}{4\pi M_s}\right]^{-1/2}, \qquad (4)$$

where L — film thickness, A — exchange stiffness, H_{pa} — perpendicular anisotropy field ($H_{pa} = 2K_p/M_s$). Using the values H_{si} obtained from the simulations, from equation (4), we find the grain fraction distribution according to the values of the magnetic perpendicular anisotropy field H_{pai}. Fig. 5 shows the simulation result according to equation *3* — black curve, the insert shows the corresponding histogram of grain distribution according to values H_{pa}. It is found that for films with a pronounced columnar microstructure, the value of the perpendicular anisotropy field for themaximum of grain size distribution H_{pa} is 1 kOe, whereas for films without columnar growth, the maximum number of grains is characterized by $H_{pa} \approx 300$ Oe on a similar distribution.

4. Conclusion

Fe-Ni–C alloy films were synthesized by chemical deposition using natural polysaccharides: arabinogalactan, starch and sucrose as reducing agents. The influence of chemical and phase composition of the coatings on the microstructure and magnetic characteristics of the synthesized samples was studied. The invar feature of the alloy Fe-Ni–C at 34% Ni manifests itself in a sharp decrease in the

values of saturation magnetization and local anisotropy field. It is shown that the main contribution to the local magnetic anisotropy of the studied coatings is made by the anisotropy of induced magnetization inhomogeneities. The correlation between the coercive force value measured at different temperatures and the stochastic domain anisotropy field has been revealed, suggesting that the H_c value is mainly determined by this anisotropy. The contribution of additional perpendicular magnetic anisotropy associated with the columnar growth of Fe-Ni−C coatings is evaluated.

Acknowledgments

The authors thank the Krasnoyarsk Regional Research Equipment Sharing Center of the Federal Research Center Krasnoyarsk Science Center of the Siberian Branch of the Russian Academy of Sciences for the provided equipment for measurements.

Funding

The study was done with financial support from the Russian Foundation for Basic Research, Government of Krasnoyarsk Territory and the Krasnoyarsk Regional Fund of Science within scientific project No. 20-43-240003.

Conflict of interest

The authors declare that they have no conflict of interest.

References

[1] T. Yamamoto, T. Nagayama, T. Nakamura. J. Electrochem. Soc. **166**, *1*, D3228 (2019).
[2] M. Theis, S. Ediger, M.T. Schmitt, J.-E. Hoffmann, M. Saumer. Phys. Status Solidi A **210**, *5*, 853 (2013).
[3] A.V. Svalov, A.V. Arkhipov, V.N. Lepalovskii, E.A. Stepanova, V.O. Vas'kovskii, G.V. Kurlyandskaya. Phys. Solid State **63**, *10*, 1553 (2021).
[4] H.L. Seet, X.P. Li, Z.J. Zhao, Y.K. Kong, H.M. Zheng, W.C. Ng. J. Appl. Phys. **97**, *10*, 10N304 (2005).
[5] Z. Zhu, H. Feng, X. Cheng, H. Xie, Q. Liu, J. Wang. J. Phys. D **51**, *4*, 045004 (2018).
[6] T. Yanai, R. Tanaka, R. Ueno, K. Mieda, J. Kaji, T. Morimura, A. Yamashita, M. Nakano, H. Fukunaga. AIP Advances **10**, *1*, 015047 (2020).
[7] B.G. Sukhov, G.P. Aleksandrova, L.A. Grishchenko, L.P. Feoktistova, A.N. Sapozhnikov, O.A. Proydakova, A.V. T'kov, S.A. Medvedeva, B.A. Trofimov. Zhurn. strukturn. khimii **48**, *5*, 979 (2007). (in Russian).
[8] M. Darques, A. Encinas, L. Vila, L. Piraux. J. Phys. D **37**, *10*, 1411 (2004).
[9] G. Herzer. Acta Materialia **61**, *3*, 718 (2013).
[10] V.A. Ignatchenko, R.S. lskhakov. JETP **45**, *3*, 1005 (1977).
[11] E.M. Chudnovsky, W.M. Saslow, R.A. Serota. Phys. Rev. B **33**, *1*, 251 (1986).
[12] R.S. Iskhakov, V.A. Ignatchenko, S.V. Komogortsev, A.D. Balaev. JETP Lett. **78**, *10*, 646 (2003).
[13] R.S. Iskhakov, S.V. Komogortsev. Phys. Met. Metallogr. **112**, **7**, 666 (2011).
[14] D.A. Velikanov. Vestn. Sib. GAU **53**, 147 (2014).
[15] E.A. Denisova, L.A. Chekanova, S.V. Komogortsev, I.V. Nemtsev, R.S. Iskhakov, M.V. Dolgopolova. J. Supercond. Nov. Magn. **34**, *10*, 2681 (2021).
[16] R.M. Bozorth. Ferromagnetism. Van Nostrand, N. Y.(1951).
[17] S.V. Komogortsev, R.S. Iskhakov. Phys. Solid State **47**, *3*, 495 (2005).
[18] A.V. Svalov, A.N. Gorkovenko, A. Larrañaga, M.N. Volochaev, G.V. Kurlyandskaya. Sensors **22**, *21*, 8357 (2022).
[19] P.N. Solovev, A.V. Izotov, B.A. Belyaev, N.M. Boev. Phys. B: Condens. Matter **604**, 412699 (2021).
[20] S.V. Komogortsev, I.G. Vazhenina, S.A. Kleshnina, R.S. Iskhakov, V.N. Lepalovskij, A.A. Pasynkova, A.V. Svalov. Sensors **22**, *9*, 3324 (2022).

Translated by Ego Translating